AD-A049 181 ROCKWELL INTERNATIONAL THOUSAND OAKS CALIF SCIENCE --ETC F/G 11/2
ACOUSTIC SURFACE WAVE SCATTERING: THE DETECTION OF SURFACE CRAC--ETC(U)
DEC 77 B T KHURI-YAKUB, A G EVANS, G S KINO N00014-76-C-0854

UNCLASSIFIED SC5064.2TR NL

| OF |
AD
A049181

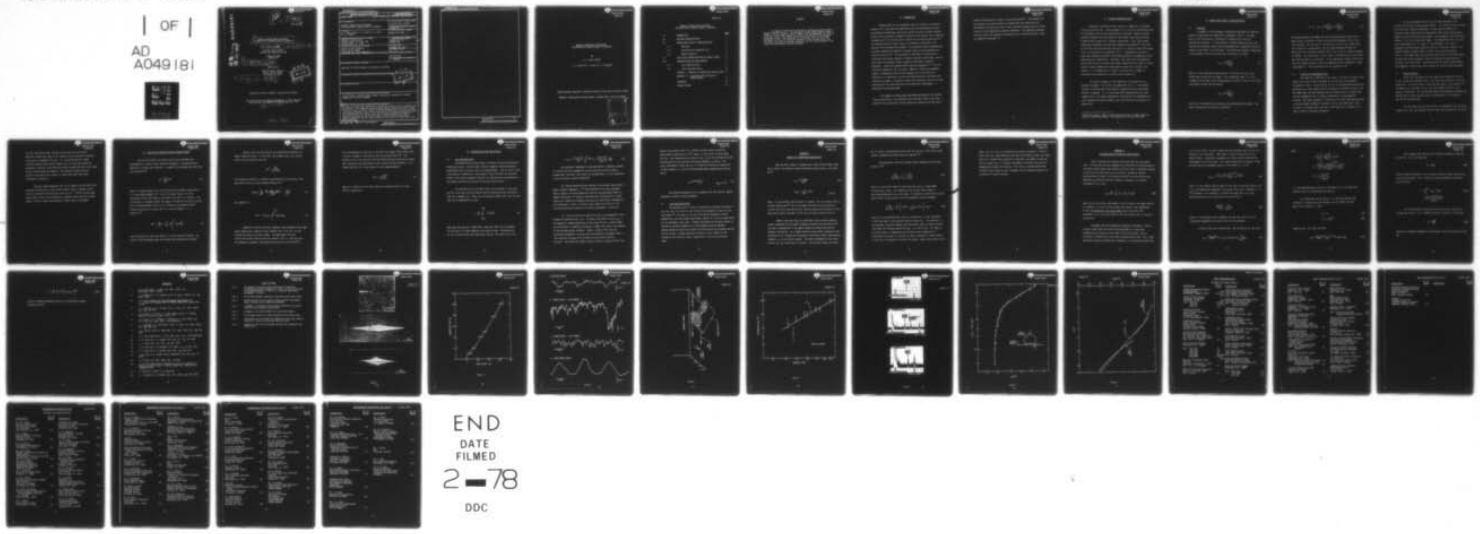

END
DATE
FILMED
2-78
DDC

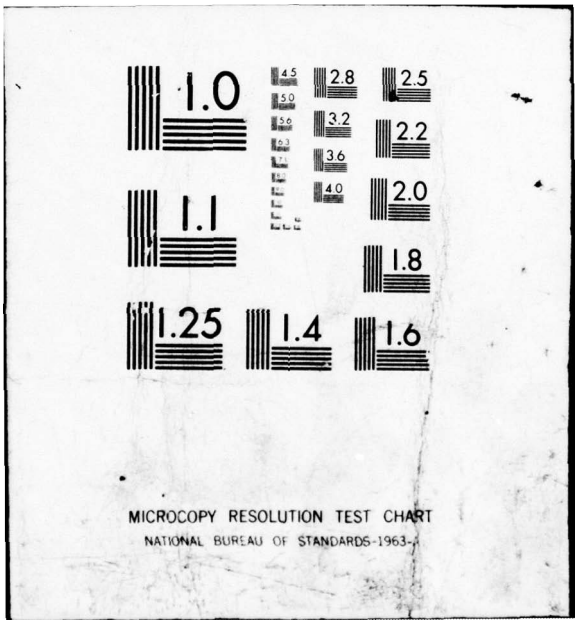
1.0
1.1
1.25
1.4
1.6
1.8
2.0
2.2
2.5
2.8
3.2
3.6
4.0
4.5
5.0
5.6
6.3
MICROCOPY RESOLUTION TEST CHART
NATIONAL BUREAU OF STANDARDS-1963-A

Rockwell International
Science Center

12

14 SC5064.2TR

COPY NO. 16

6 ACOUSTIC SURFACE WAVE SCATTERING:
THE DETECTION OF SURFACE CRACKS IN CERAMICS.

9 Technical Report. 1 Nov. 76-30 Nov 77,

11/01/76 thru 11/30/77
Contract No. N00014-76-C-0624

Project No. 471
(NR039-129)

10 B. T. /Khuri-Yakub, A. G. /Evans
G. S. /Kino B. R. /Tittmann

Submitted to:

Office of Naval Research
800 N. Quincy Street
Arlington, VA 22217

11 24 Dec 77 12 36 p.

Approved for Public Release; distribution unlimited

This Research was Sponsored by the Office of Naval Research
Under Contract No. N00014-76-C-0854 (Project No. 471)

15

389 949

UNCLASSIFIED

SECURITY CLASSIFICATION OF THIS PAGE (When Data Entered)

REPORT DOCUMENTATION PAGE		READ INSTRUCTIONS BEFORE COMPLETING FORM
1. REPORT NUMBER	2. GOVT ACCESSION NO.	3. RECIPIENT'S CATALOG NUMBER
4. TITLE (and Subtitle) ACOUSTIC SURFACE WAVE SCATTERING: THE DETECTION OF SURFACE CRACKS IN CERAMICS		5. TYPE OF REPORT & PERIOD COVERED 11/01/76 thru 11/30/77 6. PERFORMING ORG. REPORT NUMBER SC5064.2TR
7. AUTHOR(s) B. T. Khuri-Yakub, A. G. Evans, G. S. Kino, B. R. Tittmann		8. CONTRACT OR GRANT NUMBER(s) N00014-76-C-0624
9. PERFORMING ORGANIZATION NAME AND ADDRESS Rockwell International Science Center, P.O. Box 1085 Thousand Oaks, CA 91360		10. PROGRAM ELEMENT, PROJECT, TASK AREA & WORK UNIT NUMBERS Project No. 471 (NR039-129)
11. CONTROLLING OFFICE NAME AND ADDRESS Office of Naval Research 800 N. Quincy Street Arlington, VA 22217 (Code 471)		12. REPORT DATE December 20, 1977 13. NUMBER OF PAGES 30
14. MONITORING AGENCY NAME & ADDRESS(if different from Controlling Office)		15. SECURITY CLASS. (of this report) Unclassified 15a. DECLASSIFICATION/DOWNGRADING SCHEDULE

16. DISTRIBUTION STATEMENT (of this Report)

Approved for Public Release; distribution unlimited

17. DISTRIBUTION STATEMENT (of the abstract entered in Block 20, if different from Report)

18. SUPPLEMENTARY NOTES

19. KEY WORDS (Continue on reverse side if necessary and identify by block number)

surface cracks, surface acoustic waves, scattering, attenuation, fracture probability, surface roughness

20. ABSTRACT (Continue on reverse side if necessary and identify by block number)

An acoustic surface wave technique for detecting surface cracks in ceramics has been devised. The technique has been demonstrated to detect individual cracks at least as small as 60μm in depth, with the detectability limit for individual cracks being imposed by the size distribution of the adjacent background cracks. The attenuation of the surface wave has also been attributed (at least in structural ceramics) to the surface cracks, and preliminary correlations between attenuation and the large extremes of the crack size distribution have been reported.

DD FORM 1 JAN 73 1473 EDITION OF 1 NOV 65 IS OBSOLETE

UNCLASSIFIED

SECURITY CLASSIFICATION OF THIS PAGE (When Data Entered)

Rockwell International
Science Center
SC5064.2TR

ACOUSTIC SURFACE WAVE SCATTERING: THE DETECTION OF SURFACE CRACKS IN CERAMICS

By

B. T. Khuri-Yakub*

A. G. Evans,# G. S. Kino,* B. R. Tittmann#

*Edward Ginzton Laboratory, Stanford University, Palo Alto, California 96305

#Rockwell International Science Center, Thousand Oaks, California 91360

SC5064.2TR

ACOUSTIC SURFACE WAVE SCATTERING: THE DETECTION OF SURFACE CRACKS IN CERAMICS

ABSTRACT

An acoustic surface wave technique for detecting surface cracks in ceramics has been devised. The technique has been demonstrated to detect cracks at least as small as 60 μm in depth, with the detectability limit for individual cracks being imposed by the size distribution of the adjacent background cracks. The attenuation of the surface wave has also been attributed (at least in structural ceramics) to the surface cracks, and preliminary correlations between attenuation and the large extremes of the crack size distribution have been reported.

1.0 INTRODUCTION

Surface cracks are an omnipresent source of fracture in structural ceramics.[1-3] The cracks are generated during finishing operations (such as grinding and machining); and usually consist of arrays of semi-elliptical cracks, with an essentially random inclination to the surface, but a preferred alignment parallel to the direction of motion of the abrading particles.[4] The characterization of these cracks is an essential constituent in an effective failure prediction procedure. The characterization techniques that have been conventionally applied to surface cracks are dye penetrants and fracture statistics.[5] The dye penetrant techniques are restricted to relatively large cracks, because of inherent resolution limitations, and are only viable in structural ceramic systems as preliminary inspection procedures. Statistical methods exhibit superior prospects.[1,5] But the statistical approach is not, by itself, capable of identifying components subject to anomalously severe surface damage, on an individual basis. Alternative, or additional, surface crack characterization techniques must, therefore, be sought. An acoustic surface wave technique, that has the basic prerequisities for satisfying the failure prediction requirements, is described in the present paper.

Two aspects of surface wave scattering have potential for surface flaw charactrization: the scattering from individual flaws at the large extreme of the distribution, and the cumulative scattering from the entire

surface flaw population (related to the attentuation[6]). The prospects for each approach are examined herein by studying both the scattering from deliberately introduced individual cracks, and the attenuation due to various arrays of cracks generated by abrasion treatments. For comparative purposes, the crack arrays are separately characterized, on a statistical basis, using an indentation technique.[7]

2.0 SPECIMEN CHARACTERIZATION

The material selected for this study was a commercial, hot-pressed silicon nitride (NC 132). Plate specimens (3 x 3 x 0.5 cm) were machined from an as-pressed billet and one surface optically polished. Specific surface grinding treatments were then applied to each sample using 30 μm and 70 μm diamond abrasive pastes and a standard diamond wheel. Then, three surface cracks were introduced using the Knoop indentation technique.[8] The sizes of the cracks were characterized using optical or scanning electron microscopy (Fig. 1); the results are presented in Fig. 2. Subsequently, the plastic zones were removed by grinding* (the grinding condition corresponding to that applied prior to indentation). Thereafter, the cracks were not detectable, using either optical or electron microscopy, because the thin layer of surface plasticity that accompanies grinding tends to obscure the residual crack opening. It is assumed that all cracks are semicircular in shape, in accordance with observations of Petrovic and co-workers.[8]

The surface roughness of each sample was also measured using a Datatrak instrument. The results are summarized in Fig. 3. The expected increase in the amplitude of the surface irregularities with the grinding severity is apparent. It is also evident that uncharacteristically deep troughs exist in the sample subjected to a 30 μm grind (the consequence of a poorly sequenced grinding procedure)--the significance of this feature will emerge later.

---

*The plastic zone in Si_3N_4 is relatively shallow and its removal does not effect a significant change in the dimensions of the surface cracks.

3.0 SURFACE WAVE ACOUSTIC CHARACTERIZATION

3.1 Technique

A schematic of the transducer configuration developed for launching acoustic surface waves on ceramics[9] is presented in Fig. 4. A surface wave is firstly excited on a piezoelectric ($LiNbO_3$) delay line by an interdigital transducer. A fluid couplant is placed between the delay line (outside the transducer region) and the nonpiezoelectric substrate on which an acoustic surface wave is to be excited. The surface wave becomes a leaky wave in the presence of the fluid and excites a bulk wave at an angle:

$$\theta_1 = \sin^{-1}\left(\frac{v_f}{v_{SL}}\right) \tag{1}$$

where v_f is the longitudinal wave velocity in the fluid, and v_{SL} is the surface wave velocity on the $LiNbO_3$. This longitudinal wave is, in turn, arranged to be incident on the nonpiezoelectric material at the critical angle that permits surface wave excitation:

$$\theta_2 = \sin^{-1}\left(\frac{v_f}{v_{SC}}\right) \tag{2}$$

where v_{SC} is the surface wave velocity on the nonpiezoelectric medium. The angle θ between the two solids is, therefore:

$$\theta = \theta_1 - \theta_2 = \sin^{-1}\left(\frac{v_f}{v_{SL}}\right) - \sin^{-1}\left(\frac{v_f}{v_{SC}}\right) \quad (3)$$

The distance between the $LiNbO_3$ line and the nonpiezoelectric delay line is made as small as possible in order to minimize the propagation loss in the fluid couplant. For the case of a surface wave on the Y-Z cut $LiNbO_3$ delay line, coupled to a Si_3N_4 ceramic, the calculated maximum efficiency (of 54%) occurs for an overlay distance ℓ (Fig. 4) of .5 mm, at a center frequency of 100 MHz. This constitutes a loss of about 2.7 dB conversion of the surface wave from one material to the other. In our experiments, glycerol was used as the fluid couplant because it does not evaporate quickly and because it forms a good meniscus. The inclination θ for this couplant is 13^o.

3.2 Insertion and Propagation Loss

The reduction in amplitude of the signal reflected at the edge of the sample can be used to obtain estimates of the insertion and propagation (attenuation) losses. The two sources of loss are distinguished by performing experiments on a given sample with the transducer at different distances from the sample edge, and then presuming that the insertion loss is constant and that the propagation loss is linearly proportional to the propagation distance. The latter assumption is justified on the basis that beam spreading at the wavelengths (30-60 μm), distances (1-2 cm), and beam widths (1 mm) involved is negligably small, and that a sufficient area is sampled by the beam to ensure a consistent attenuation.

The loss experiments have thus far only been completed on the polished 9 μm and 30 μm diamond ground samples. The insertion loss was found to be relatively frequency independent (in the range 80-130 MHz); but increased as the surface condition degenerated, from ~4 dB on the polished sample to ~9 dB on the 30 μm ground sample. The propagation loss results are plotted in Fig. 5 for the polished sample. The attenuation level is low and varies approximately as λ^{-4}, where λ is the wavelength. The results obtained on the 30 μm ground sample are similar in character, except at the highest frequency (130 MHz) where no return signal could be detected. Finally, it was noted that finely polishing the surface of the ground samples to remove the surface roughness, without disrupting the underlying crack structure, had little effect: and certainly did not restore the attenuation and propagation losses to the values obtained for the fully polished sample.

3.3 Defect Detection

Cracks were introduced into each sample using indentation loads of 10, 20, and 40 N corresponding (Fig. 2) to crack radii of 60, 80, and 120 μm, respectively. The crack planes in each case were normal to the long axis of the sample; this coincides, in turn, with the incident direction of the acoustic surface wave. For the polished sample, the background scattering was minimal and all cracks could be clearly distinguished, as illustrated in Fig. 6a for the 60 μm crack.

For the sample with the 30 μm finish, the background level increased markedly (Fig. 6b), and although distinct signals were obtained for the 80 μm

(Fig. 6b) and 120 μm cracks, the 60 μm crack could not be discerned. Additional signals that could not be related to the deliberately introduced cracks were also apparent (Fig. 6b). It is recalled that this sample contained unusually deep surface troughs (Fig. 3), which may signify the presence of relatively large underlying cracks introduced during a prior stage of the surface preparation sequence. The additional signals are thus plausibly explained by the presence of large cracks other than those introduced by indentation.

The even larger background level on the sample with the 70 μm finish prevented the detection of both the 60 and 80 μm cracks, although a clear signal was obtained from the 120 μm crack (Fig. 6c). Finally, on the rough ground sample, none of the deliberately introduced cracks could be isolated. However, distinct signals were apparent in other areas of the sample.

4.0 STATISTICAL CHARACTERIZATION OF SURFACE CRACKS

The size distribution of surface cracks can be characterized experimentally in terms of their effective strength S: the applied stress required to initiate crack extension. In general, the strength and crack size are related by:[10]

$$S^2 = \frac{EG_c}{Y^2 a} F(\theta) \tag{4}$$

where E is Young's modulus, G_c is the critical strain energy release rate, Y is a crack shape parameter ($Y^2 = 4(1-\nu^2)$ for penny cracks), θ is the inclination of the crack plane to the stress axis, and F is a function. The distribution of strengths g(S)dS, the number of flaws per unit area of surface with a strength between S and S + dS is related to the probability Φ of fracture occurring at a stress level S in an areal element A. In general,[1,7]

$$\Phi = 1 - \left[\exp \; -\int_A dA \int_0^S g(S)dS \right] \tag{5}$$

The distribution of flaw sizes, g(a)da, is in turn related to g(S)dS: the precise relation depending upon the strength test configuration employed.

Surface crack size distributions are conveniently obtained using sphere indentation tests. In this test, the strength level, S_{TC}, and the crack size are related by (eq. A3):

$$S_{TC}^2 = \frac{EG_c}{4(1-\nu^2)a} \quad ,$$

the strength distribution is related to the cumulative distribution of the peak tensile stress at crack formation $\Phi(S_m)$ by:(7)

$$g(S_{TC}) = \frac{S_m}{\pi R^2} \quad \frac{\Phi''(1-\Phi) + (\Phi')^2}{(1-\Phi)^2} \quad = \frac{S_m \epsilon''}{\pi R^2} \tag{6}$$

and (Appendix I):

$$G(a) \sim 2\, G(S_{TC}) = \int_0^{S_{TC}} g(S_{TC})\, dS_{TC} \tag{7}$$

Indentation fracture data have, therefore, been obtained on the rough ground sample using a spherical steel indenter (Fig. 7) (cf ref. 11) and analyzed according to the above scheme. The approximate flaw size distributions derived from the data are plotted in Fig. 8. The flaw sizes were computed by assuming a polycrystalline value for G_c (80 Jm^{-2});(12)

this overestimates the flaw size in the small size regime ($\lesssim 5\,\mu$m radius) when a smaller (although ill-defined) G_c would be more pertinent.[10] Also plotted in Fig. 8 are the flaw size distribution derived from uniaxial flexure data, obtained on the same material with a similar surface condition. It is evident that G(a) for a wide range of a can be approximated by:

$$G(a) \approx G_o \left(\frac{a_o}{a}\right)^p \tag{8}$$

where a_o is taken to be $1\,\mu$m and p and G_o are constants equal to 3.3 and 10^9 m^{-2}, respectively.

5.0 INTERPRETATIONS AND IMPLICATIONS

5.1 Loss Characteristics

The attenuation of surface waves in ceramics can derive from several scattering sources: surface cracks, surface roughness, and microstructural constituents (such as grains, pores, and second phases). The low level of the microstructural attenuation in hot-pressed silicon nitride[6] and the minor effect of the surface roughness (Section 3.2) indicate that the attenuation in the present studies derives primarily from the surface cracks.

The attenuation due to surface cracks can be related, in the usual way,[6] to the crack size distribution and the scattering cross section $\Omega(a)$ (derived in Appendix II). Hence, for the long wave length limit, eqs. (8) and (A14) can be combined[6] to yield:

$$\alpha = \frac{\kappa}{\lambda^5} \int_{a_{min}}^{a_{max}} g(a) a^6 da \qquad (9)$$

where a_{max} and a_{min} are, respectively, upper and lower flaw size bounds for the area A of surface sampled by the acoustic beam. Differentiating eq. (8) to obtain g(a)da and substituting into eq. (10) gives (for $p < 6$):

$$\alpha(\lambda,a) \approx \frac{p\, G_o\, \kappa\, a_o^{\,p}}{\lambda^5} \int_0^{\infty} a^{5-p}\, da = \frac{p\, G_o\, \kappa\, a_o^{\,p}}{(6-p)\,\lambda^5}\, a_{max}^{6-p} \qquad (10)$$

The substantial dependence on the upper bound is important, because it indicates that the propagation loss may correlate with the fracture strength when individual flaws cannot be distinguished (c.f. bulk attenuation in coarse grained or porous ceramics[6]).

The limited attenuation data obtained in the present study exhibit a weaker frequency dependence (λ^{-4}) than predicted by the long wavelength theory; probably indicating departures from the long wavelength regime, as commonly encountered in studies of microstructure attenuation.[6] Further studies will examine the frequency and crack size distribution dependence of the attentuation in detail, to obtain direct comparisions with eq. (11) (including theoretical extensions to shorter wavelengths, if possible).

It is also instructive to explore the crack size dependence of the attenuation predicted by eq. (11). The total crack density, $G(a)_{a \to a_o}$, is not expected to change appreciably as the surface finish is varied; rather, the distribution is expected to displace to larger flaw sizes as the severity of the grinding process increases. Hence, in terms of the flaw size distribution parameters, G_o and a_o would be essentially unchanged, while p would decrease (and a_{max} would increase) as the grinding severity increases. By analogy with impact fracture studies on ceramics,[13,14] the

depth of the surface cracks for a constant grinding velocity should be approximately proportional to $r^{4/3}$, where r is the radius of the grinding particle. This proportionality allows p in eq. (11) to be correlated with the grinding particle size and the distribution parameters a_o and G_o. For cracks considerably larger than a_o, p is found to be relatively insensitive to small changes in r, and the following approximate proportionality should apply:

$$\alpha \tilde{\propto} r^{(8-4p/3)} \Big/ \lambda^{5} \qquad (a_{max} >> a_o) \qquad (11)$$

The predicted dependence will be compared with loss data for samples subjected to several surface treatments.

5.2 Crack Characterization

The detectability of a crack is determined by the power scattered by the crack (eq. 9), relative to the insertion and propagation losses and the input power.[5] The theory is not yet sufficiently developed to predict detectability, but the present observations (Section 3.7) yield an upper bound for the detectable crack sizes: ranging from $<60\ \mu m$ for polished surfaces to $<120\ \mu m$ for surfaces subjected to a $70\ \mu m$ diamond grinding treatment. Improved detection should be realized by optimizing both the frequency and the overlay distance, through quantitative studies of their effects on the attenuation and insertion losses, respectively, vis-a-vis the scattered power.

APPENDIX I

ANALYSIS OF INDENTATION FRACTURE DATA

When an elastic sphere is pressed onto a semi-infinite elastic body with a force P, the surface stresses outside the contact zone, a, are given by:(7)

$$\sigma_{rr} = \frac{P\,(1-2\nu)}{2\pi r^2} \qquad \text{(A1)}$$

$$\sigma_{\theta\theta} = -\frac{P}{2\pi r^2}\,(1-2\nu) \qquad (r \gg R)$$

where r is the distance from the center of contact. For this stress field, it has been demonstrated(7) that the strength distribution for pre-existing surface flaws can be derived directly from the cumulative distribution of the peak tension $S_m (=P(1-2\nu)/2\pi R^2)$ at the crack activation condition (eq. 6).

However, when such tests are performed on high strength ceramics, plastic deformation of the sphere frequently precedes crack activation.(11) The onset of deformation in the sphere changes the contact area and the pressure distribution. For indenter materials which exhibit substantial work hardening, we will assume that the pressure distribution remains approximately parabolic, as in the elastic problem. The spatial dependence of the stress given by eq. (A1) would then still pertain. But now the contact area could

not, of course, be determined directly from the load (as in the elastic case); instead, independent evaluation would be required.(11)

The propagation condition for penny-cracks subjected to multi-axial stress is:(15)

$$\frac{E\,G_c}{4(1-\nu^2)a} = \sigma_n^2 + \frac{4\tau_m^2}{(2-\nu)^2} \qquad \text{(A2)}$$

where σ_n is the stress normal to the crack plane and τ_m is the maximum in-plane shear stress. For indentation, the surface stress state is equi-tension/compression (eq. A1); hence, if attention is restricted to cracks nearly normal to the surface, the crack propagation condition becomes:

$$\frac{E\,G_c}{4(1-\nu^2)a} = S_{TC}^2 \left[\cos^2 2\alpha + \frac{4}{(2-\nu)^2} \sin^2 2\alpha \right] \approx S_{TC}^2 \qquad \text{(A3)}$$

where S_{TC} is the applied stress level of fracture and α is the inclination of the flaw normal to the principal tensile stress axis. This condition is only expected to pertain, however, when the normal stress is tensile and the crack faces can displace without friction, i.e., for $\alpha \leq \pi/4$. At larger α, the normal stress is compressive and the shear stress (especially in polycrystalline ceramics) is unlikely to lead to substantial intensification of the crack tip because of frictional resistance. Hence, only cracks in the

range, $-\pi/4 < \alpha < \pi/4$, are considered to be prone to extension. Since all flaws within this range experience the same crack extension force, the simple result for a random flaw orientation is that G(a), the number of flaws per unit are larger than a is $\sim 2G(S_{TC})$, the number of flaw per unit are with a indentention strength less than S_{TC}. This result is modified when flaws inclined to the surface are also included, but this complexity need not be considered for present purposes.

APPENDIX II

SCATTERING CROSS SECTIONS OF SURFACE CRACKS

We will consider the situation that occurs when the crack depth $a \ll \lambda$. In this case, the main component of scattering of the surface waves is into other surface waves; the scattering into bulk waves is negligable because of the relatively weak coupling to the surface. We employ a general scattering matrix formula first derived by Kino[16] for the relative wave amplitude s_{21} scattered from one transducer (transducer 1) to another (transducer 2) by a void:

$$s_{21} = \frac{i\omega}{4} \int_S (u_i)_1 \, (\sigma_{ij}{}^i)_2 \, \eta_j dS \qquad \text{(A4)}$$

where $(u_i)_1$ is the surface displacement at the flaw due to unit power emitted by transducer 1, $(\sigma_{ij}{}^i)_2$ is the incident wave stress in the neighborhood of the flaw without the flaw being present due to unit power from transducer 2, η_j is the crack normal to the flaw surface, and S is the flaw surface area.

We suppose that the transmitting transducer (transducer 1) emits a straight crested wave (the surface wave equivalent of a plane wave) propagating at an angle θ_1 to the normal to the flaw surface. We are interested in determining to total power scattered by the flaw. This is most conveniently found by assuming that transducer 2 is of width W_2 and the flaw

is in its far field. We shall assume that this transducer has its axis at an angle θ_2 to the flaw normal. This normal is taken to be parallel to the sample surface. Elastostatic assumptions can now be used to calculate the displacements of the flaw faces. For a penny shaped crack of radius a it may be shown that the displacement normal to the surface u_o , is:[17]

$$u_{on} = \pm \frac{(T)_1 \ (1-\nu) \ (a^2-r^2)^{1/2} \cos \theta_1}{\pi \mu} \tag{A5}$$

where r is the distance from the center of the crack, μ the shear modulus, and $(T)_1$ is the longitudinal component of the stress field due to transducer 1, at the transducer. For transducer 2, Auld[12] has shown that, for a wave emitted along the z axis, the stress in the far field is:

$$\frac{(\sigma_{zz}{}^{i})_2}{(T)_2} = \frac{W_2}{(\lambda R)^{1/2}} \tag{A6}$$

where R is the distance of the transducer from the flaw, and $(T)_2$ is the longitudinal component of the stress field at the transducer.

It then follows after inserting eqs. (A5) and (A6) in eq. (A4) that:

$$s_{21} = \frac{i\omega(1-\nu)a^3}{6\mu} (T)_1 \ (T)_2 \cos \theta_1 \cos \theta_2 \frac{W_2}{(\lambda R)^{1/2}} \tag{A7}$$

where

$$A = \frac{\mu^2}{v_R}\left[1 - \left(\frac{v_S}{v_1}\right)^2\right] f_z^{\,3}\,\omega^{1/2} \tag{A8}$$

$$f_z = \frac{4\eta\left[1 - (v_R/v_S)^2\right]^{3/2}}{3\eta - 2\eta\,(v_R/v_S)^2 - 1}\left(\frac{v_S}{v_R}\right)^2$$

$$\eta^2 = \frac{1 - (v_R/v_1)^2}{1 - (v_R/v_S)^2}$$

v_1 is the longitudinal wave velocity in the medium, v_S is the shear wave velocity, and v_R is the Rayleigh wave velocity.

For convenience, we now set $P_R = 1$ for the wave emitted from transducer 1, assuming that the transducer has unit width, and take $W_2 P_R = 1$ for transducer 2. Then:

$$(T)_1 = A \tag{A9}$$

$$(T)_2 = A/W_2^{\,1/2} \tag{A10}$$

Combining eqs. (A7), (A8), and (A9):

$$s_{21} = \frac{i\omega(1-\nu)a^3}{6\mu}\left(\frac{1}{\lambda R}\right)^{1/2} A^2 \cos\theta_1 \cos\theta_2 \tag{A11}$$

We now suppose that the receiving transducer subtends an angle $d\theta_2$ at the flaw. Then it follows that:

$$W_2 = Rd\theta_2 \tag{A12}$$

The total power reradiated by a unit incident intensity signal from the flaw can now be calculated: this is defined as the one-dimensional scattering cross section Ω:

$$\Omega = \int_0^{2\pi} |s_{21}|^2 \, Rd\theta_2 \tag{A13}$$

$$= \frac{\pi\omega^2(1-\nu)^2 a^6 A^4 \cos^2\theta_1}{36\,\mu^2\lambda}$$

The flaw orientation distribution can now be used to obtain the average cross section. For a random orientation, $\langle\cos^2\theta_1\rangle = 0.5$ and hence,

$$\Omega = \frac{2\kappa a^6}{\lambda^5} \tag{A14}$$

where κ is a parameter dependent on the Poisson's ratio of the material given by:

$$\kappa = \frac{\pi^5}{9} f_z^2 (1-\nu)^2 \left[1-(v_s/v_l)^2\right]^4 \qquad \text{(A15)}$$

A similar frequency dependence pertains to scattering by surface irregularities.(18)

REFERENCES

1. A. G. Evans and R. L. Jones, Jnl. Amer. Ceram. Soc., March/April 1978, in press

2. J. J. Mecholsky, S. W. Freiman, and R. W. Rice, J. Mater. Sci., 11, 1310, 1976

3. R. W. Rice, Ceramics for High Performance Applications (ed. J. J. Burke, A. E. Gorum, and R. N. Katz), Brook Hill, March 1974, p. 287

4. J. J. Mecholsky, S. W. Freiman, and R. W. Rice, Jnl. Amer. Ceram. Soc., 60, 116, 1977

5. A. G. Evans, G. S. Kino, B. T. Khuri-Yakub, and B. R. Tittmann, Materials Evaluation, April 1977, p. 85

6. A. G. Evans, B. R. Tittmann, L. Ahlberg, B. T. Khuri-Yakub, and G. S. Kino, Jnl. Appl. Phys., to be published

7. J. R. Matthews, F. A. McClintock, and W. A. Shack, Jnl. Amer. Ceram. Soc., 59, 304, 1976

8. J. J. Petrovic and M. G. Mendiratta, Jnl. Amer. Ceram. Soc., 59, 163, 1976

9. B. T. Khuri-Yakub and G. S. Kino, Appl. Phys. Lett., to be published

10. A. G. Evans and T. G. Langdon, Prog. Mat. Sci., 21, 171, 1976

11. F. F. Lange, Intl. Jnl. Frac., 12, 409, 1976

12. A. G. Evans and S. M. Wiedehorn, Jnl. Mater. Sci., 9, 270, 1974

13. A. G. Evans and T. R. Wilshaw, Acta. Met., 24, 939, 1976

14. A. G. Evans, M. E. Gulden, and M. Rosenblatt, Proc. Roy. Soc., in press

15. A. G. Evans, Jnl. Amer. Ceram. Soc., in press

16. G. S. Kino, "Application of Reciprocity Theory to Scattering of Acoustic Waves by Flaws," G. 02742, Ginzton Lab, Stanford Univ. (September 1977)

17. B. Auld and G. Elston, to be published

18. R. C. Steg and P. G. Klemens, Phys. Rev. Letters, 24, 381 (1970)

FIGURE CAPTIONS

Fig. 1 Micrographs of surface cracks introduced by indentation: (a) scanning electron micrograph, P = 20 N, (b) polarized light reflected micrograph, P = 50 N, (c) reflected light optical micrograph, P = 110 N.

Fig. 2 The relation between indentation load and surface crack radius.

Fig. 3 Surface profiles of the various surfaces used in the present study, obtained using a Datatrak instrument.

Fig. 4 A schematic illustrating the transducer configuration used for launching high frequency surface waves.

Fig. 5 Propagation loss data obtained for the polished sample.

Fig. 6 Oscilloscope records of signals obtained from surface cracks.

Fig. 7 The probability of fracture for indentation using steel spheres, plotted as a function of the peak tensile stress.

Fig. 8 Cumulative flaw size distribution derived from indentation and flexure data.

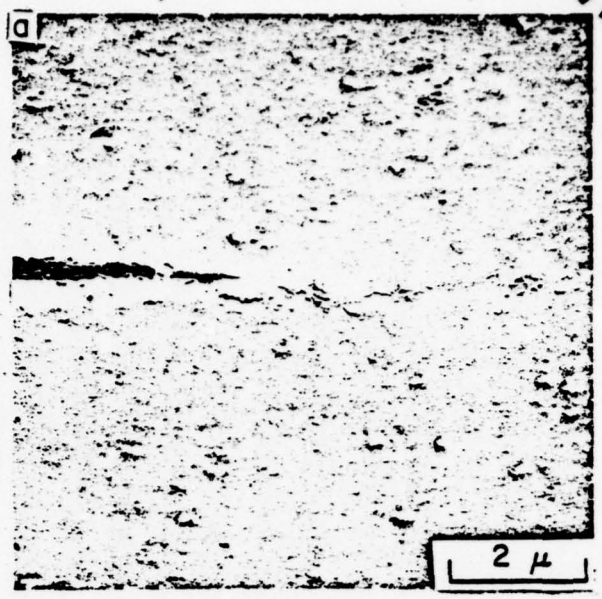

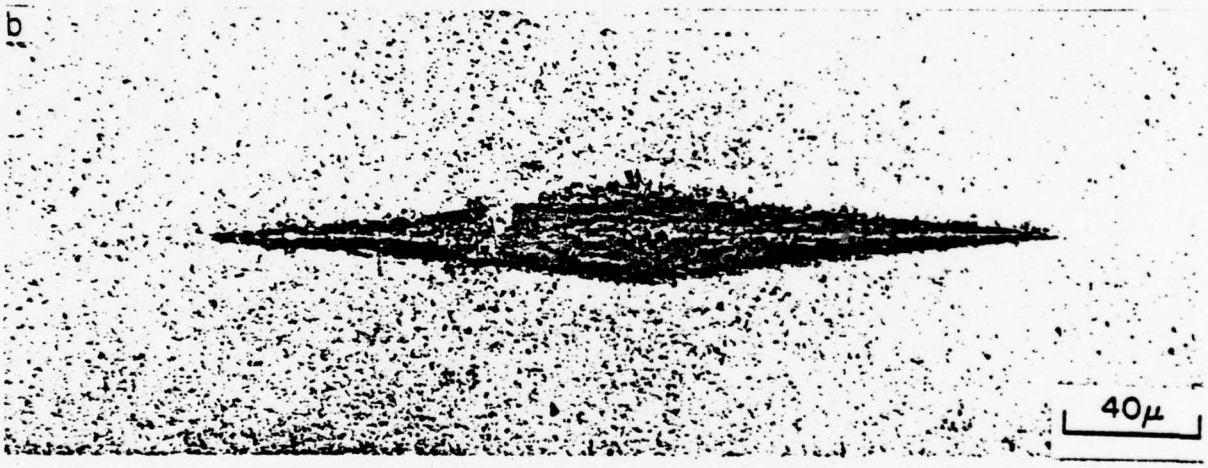

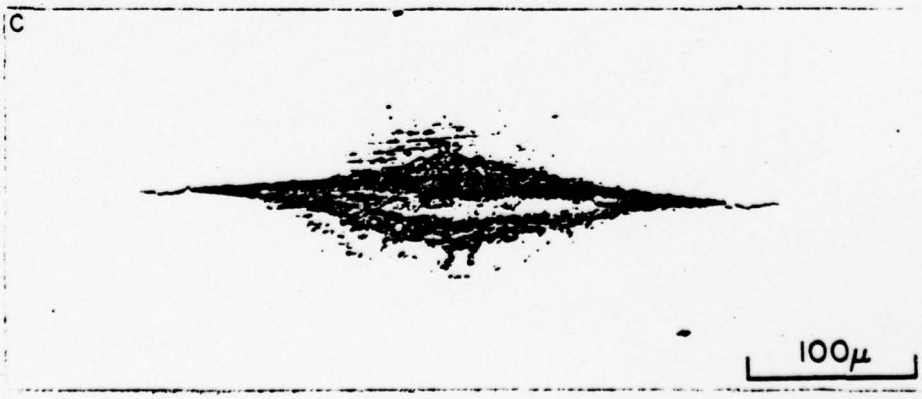

Figure 1

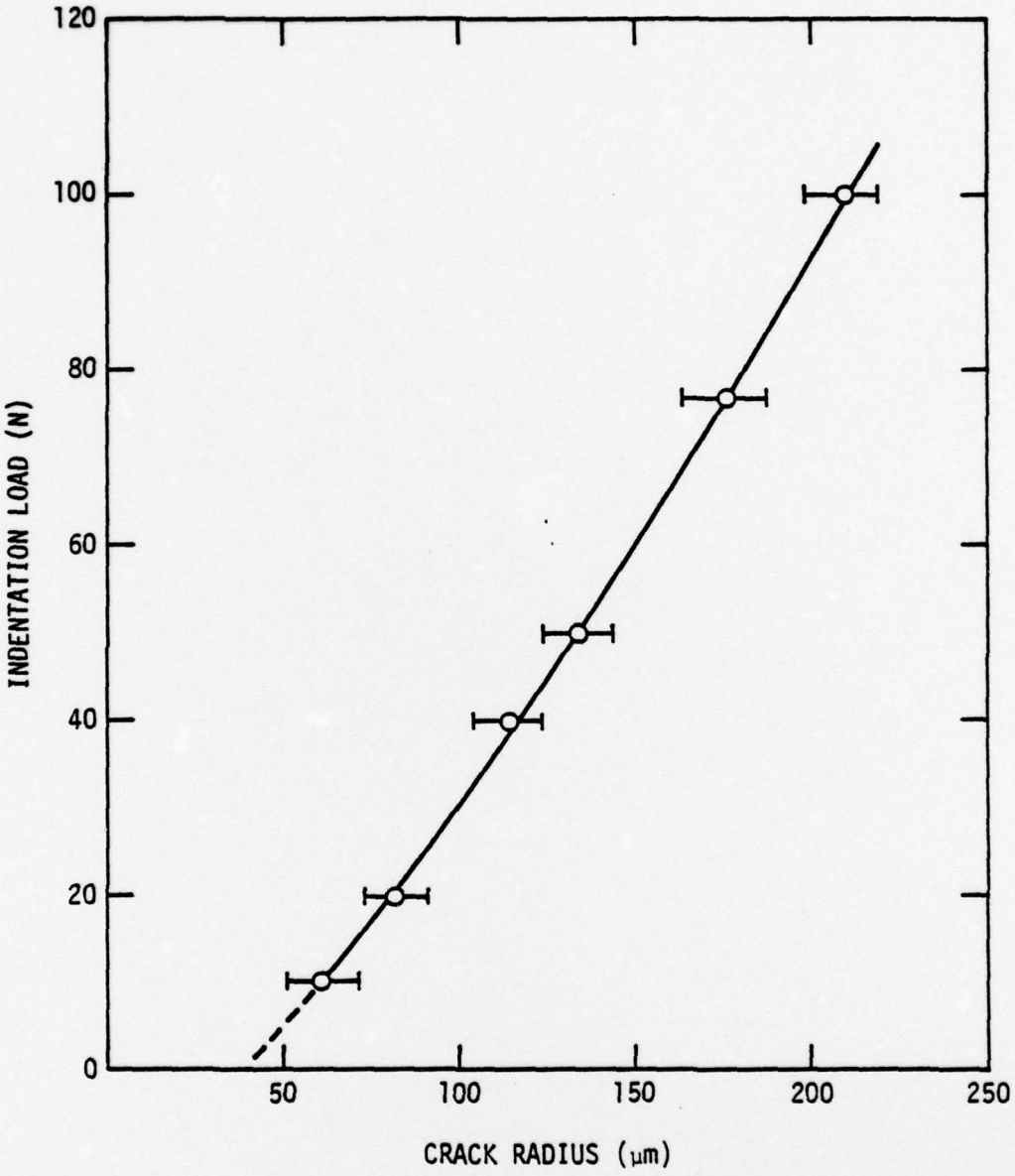
120
100
80
60
40
20
0
INDENTATION LOAD (N)
50
100
150
200
250
CRACK RADIUS (μm)

Figure 2

a) POLISHED SAMPLE

b) GROUND SAMPLE - 30μm DIAMOND

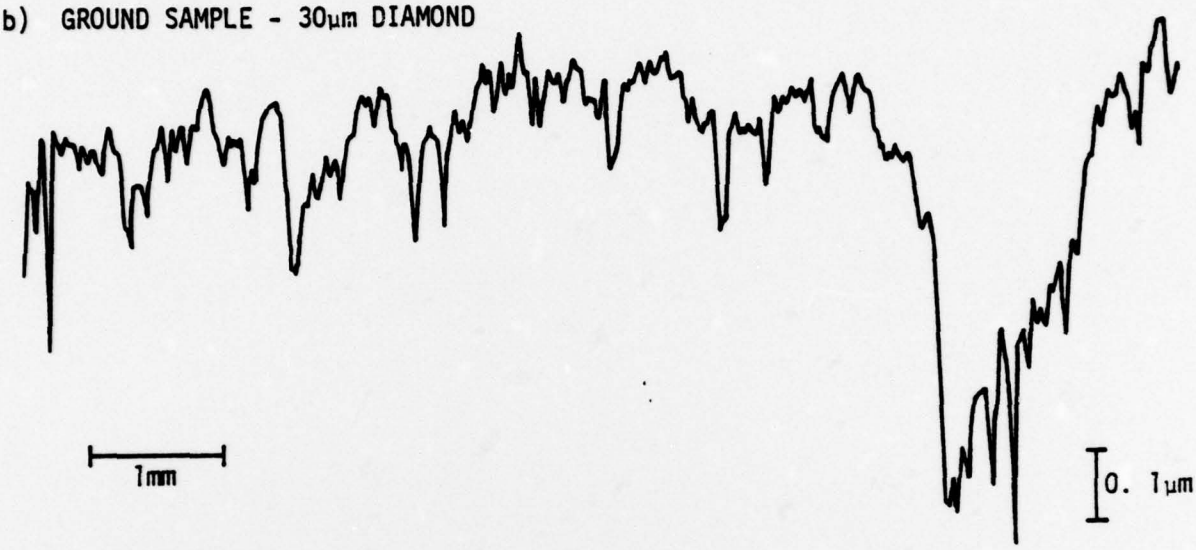

c) GROUND SAMPLE - 70μm DIAMOND

d) ROUGH GROUND SAMPLE

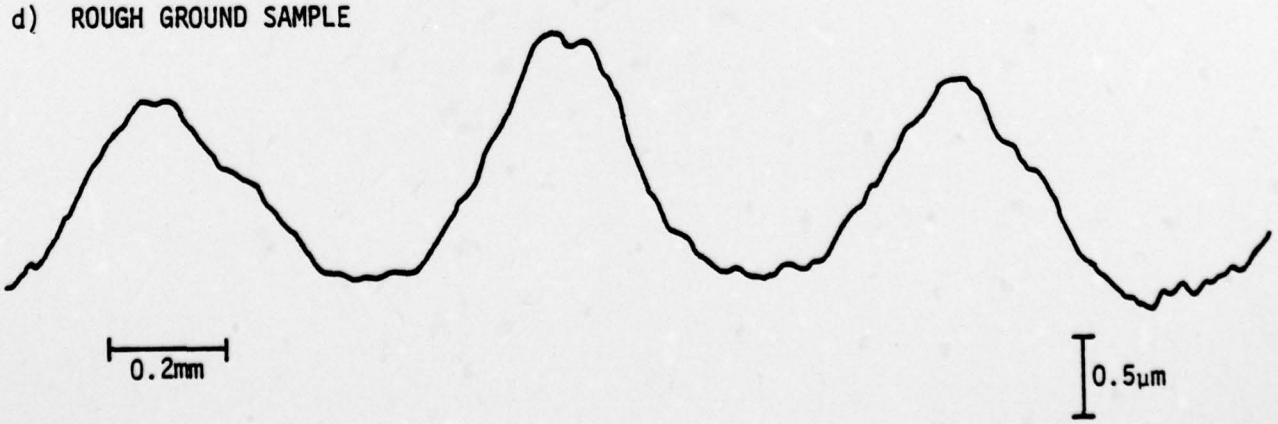

Figure 3

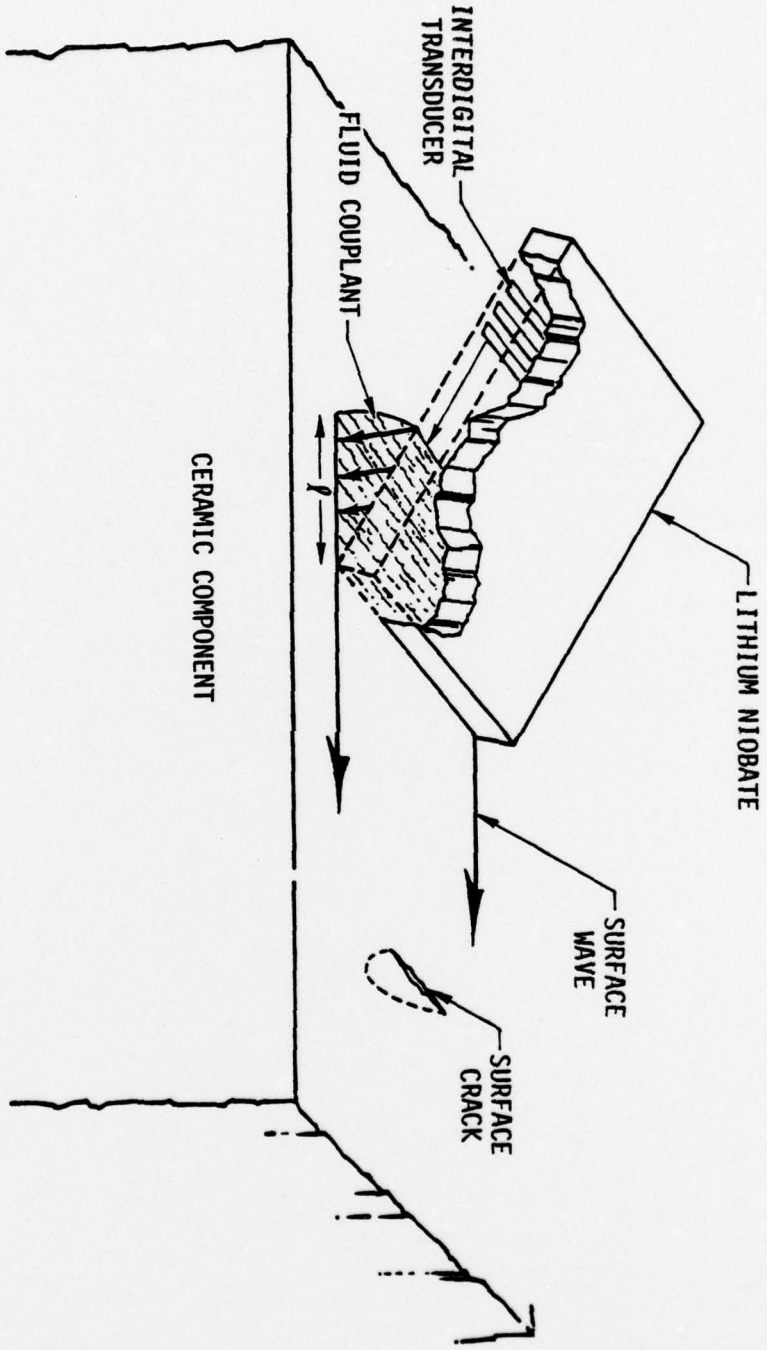
INTERDIGITAL TRANSDUCER
FLUID COUPLANT
CERAMIC COMPONENT
LITHIUM NIOBATE
SURFACE WAVE
SURFACE CRACK

Figure 4

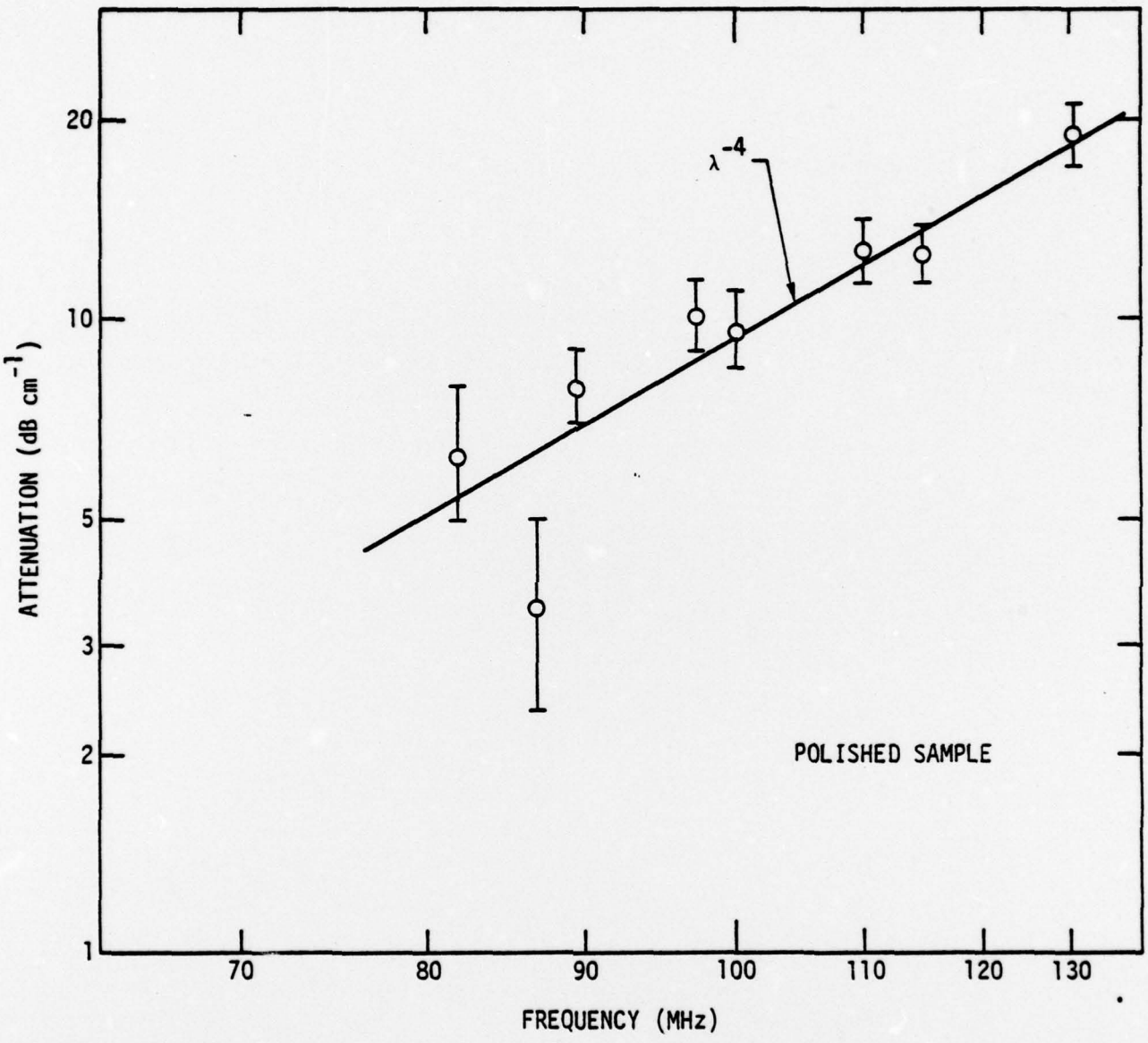
20
10
5
3
2
1
ATTENUATION (dB cm^{-1})
λ^{-4}
POLISHED SAMPLE
70
80
90
100
110
120
130
FREQUENCY (MHz)

Figure 5

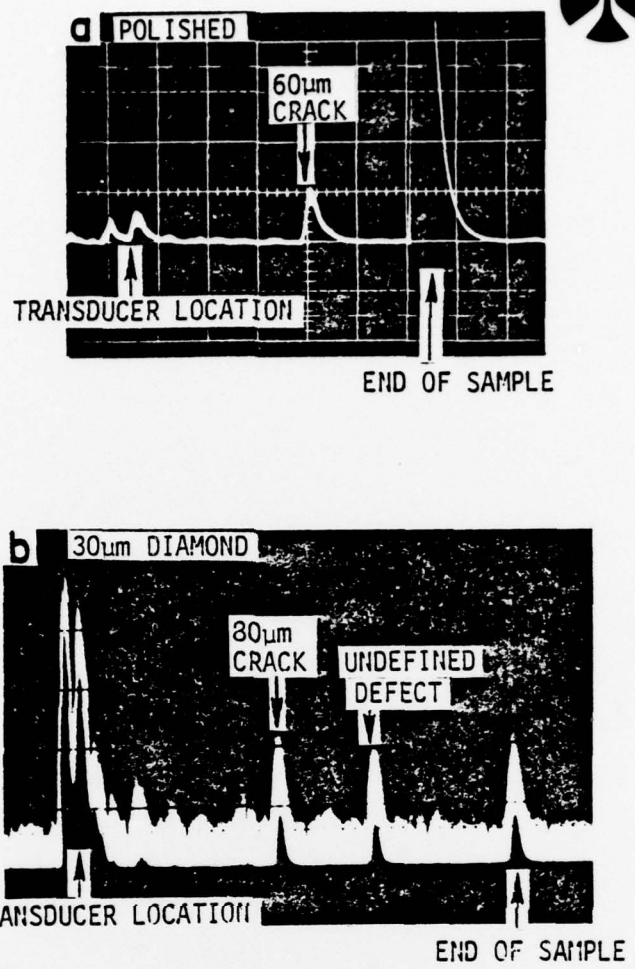
a
POLISHED
60μm
CRACK
TRANSDUCER LOCATION
END OF SAMPLE
b
30μm DIAMOND
80μm
CRACK
UNDEFINED
DEFECT
TRANSDUCER LOCATION
END OF SAMPLE
c
70μm DIAMOND
120μm
CRACK
TRANSDUCER LOCATION
END OF SAMPLE

Figure 6

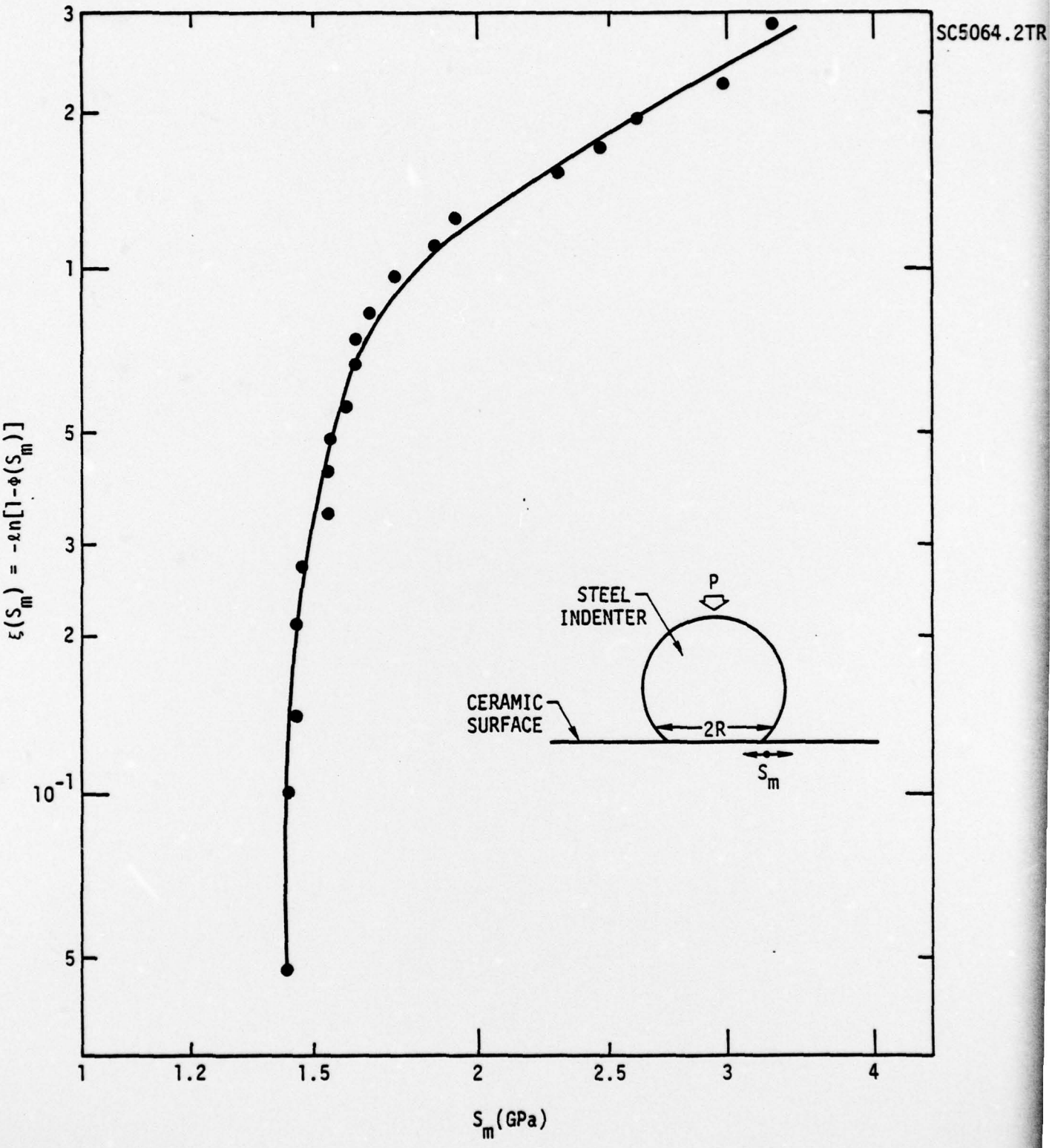
SC5064.2TR
$\xi(S_m) = -\ln[1-\phi(S_m)]$
3
2
1
5
3
2
10^{-1}
5
1
1.2
1.5
2
2.5
3
4
S_m(GPa)
STEEL INDENTER
P
CERAMIC SURFACE
2R
S_m

Figure 7

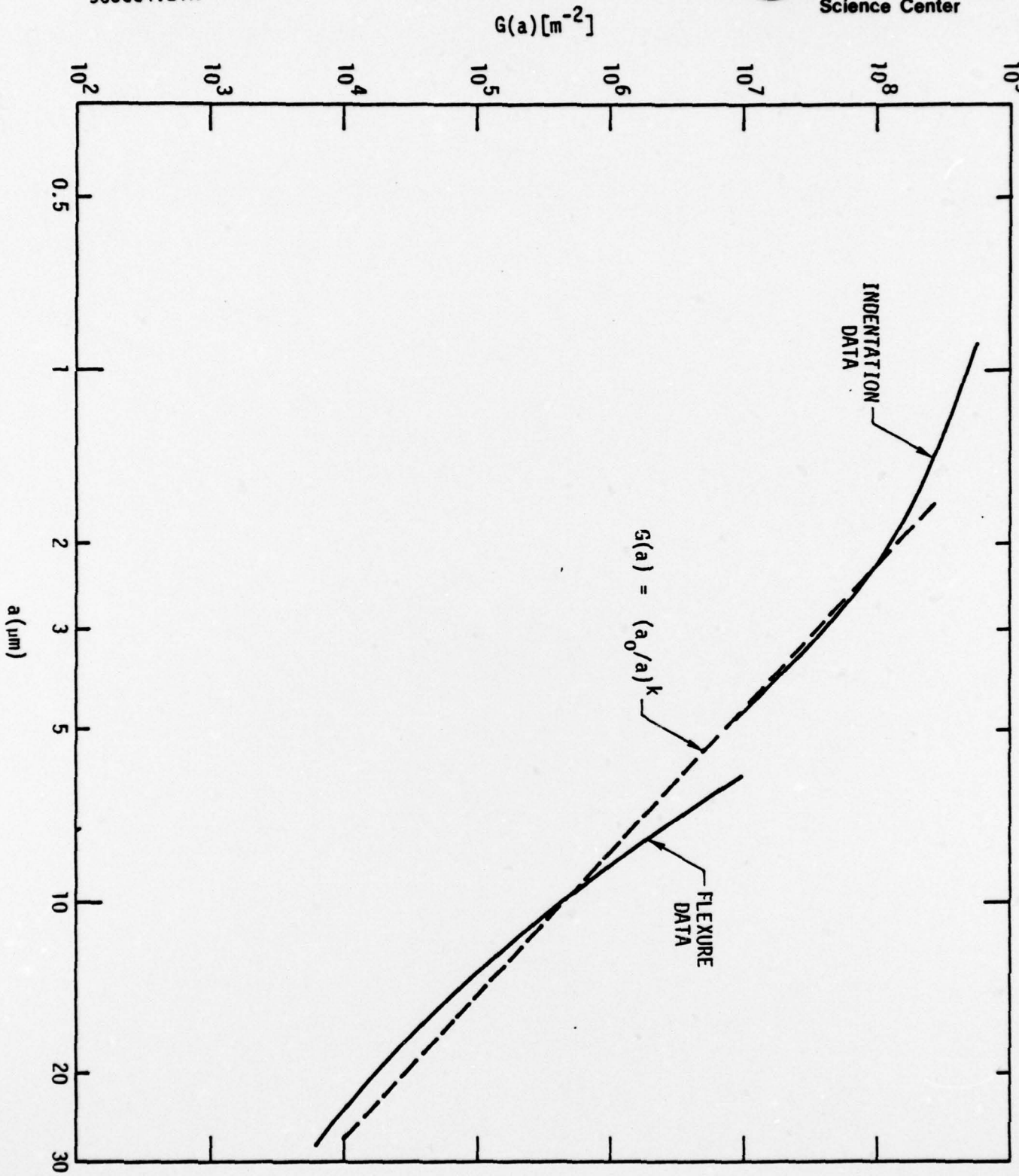
G(a)[m^{-2}]
10^2
10^3
10^4
10^5
10^6
10^7
10^8
10^9
a(μm)
0.5
1
2
3
5
10
20
30
INDENTATION DATA
G(a) = $(a_o/a)^k$
FLEXURE DATA

Figure 8

BASIC DISTRIBUTION LIST

October 1976

Technical and Summary Reports

Organization	No. of Copies
~~Defense Documentation Center~~ ~~Cameron Station~~ ~~Alexandria, Virginia 22314~~	Shown ~~(12)~~ on Cover
Office of Naval Research Department of the Navy Arlington, VA 22217	Shown
Attn: ~~Code 471~~	~~(1)~~ on
Code 102	(1) Cover
Code 470	(1)
Commanding Officer Office of Naval Research Branch Office 495 Summer Street Boston, Massachusetts 02210	(1)
Commanding Officer Office of Naval Research Branch Office 536 South Clark Street Chicago, Illinois 60605	(1)
Office of Naval Research San Francisco Area Office One Hallidie Plaza - Suite 601 San Francisco, California 94102	
Attn: Dr. P. A. Miller	(1)
Naval Research Laboratory Washington, D.C. 20390	
Attn: Code 6000	(1)
Code 6100	(1)
Code 6300	(1)
Code 6400	(1)
~~Code 2627~~	~~(1)~~ Shown on Cover
Naval Air Development Center Code 302 Warminster, Pennsylvania 18974	
Attn: Mr. F. S. Williams	(1)
Naval Air Propulsion Test Center Trenton, New Jersey 08628	
Attn: Library	(1)
Naval Construction Batallion Civil Engineering Laboratory Port Hueneme, California 93043	
Attn: Materials Division	(1)
Naval Electronics Laboratory Center San Diego, California 92152	
Attn: Electron Materials Sciences Division	(1)
Naval Missile Center Materials Consultant Code 3312-1 Point Mugu, California 93041	(1)
Commanding Officer Naval Surface Weapons Center White Oak Laboratory Silver Spring, Maryland 20910	
Attn: Library	(1)
David W. Taylor Naval Ship R&D Center Materials Department Annapolis, Maryland 21402	(1)
Naval Undersea Center San Diego, California 92132	
Attn: Library	(1)
Naval Underwater System Center Newport, Rhode Island 02840	
Attn: Library	(1)
Naval Weapons Center China Lake, California 93555	
Attn: Library	(1)
Naval Postgraduate School Monterey, California 93940	
Attn: Mechanical Engineering Dept.	(1)
Naval Air Systems Command Washington, D.C. 20360	
Attn: Code 52031	(1)
Code 52032	(1)
Code 320	(1)

Organization	No. of Copies
Naval Sea Systems Command Washington, D.C. 20362 Attn: Code 035	(1)
Naval Facilities Engineering Command Alexandria, Virginia 22331 Attn: Code 03	(1)
Scientific Advisor Commandant of the Marine Corps Washington, D.C. 20380 Attn: Code AX	(1)
Naval Ship Engineering Center Department of the Navy CTR BG #2 3700 East-West Highway Prince Georges Plaza Hyattsville, Maryland 20782 Attn: Engineering Materials and Services Office, Code 6101	(1)
Army Research Office Box CM, Duke Station Durham, North Carolina 27706 Attn: Metallurgy & Ceramics Div.	(1)
Army Materials and Mechanics Research Center Arsenal Street Watertown, Massachusetts 02172 Attn: Res. Programs Office (AMXMR-P)	(1)
Air Force Office of Scientific Research Bldg. 410 Bolling Air Force Base Washington, D.C. 20332 Attn: Chemical Science Directorate Electronics and Solid State Sciences Directorate	(1) (1)
Air Force Materials Lab (MX) Wright-Patterson AFB Dayton, Ohio 45433	(1)
NASA Headquarters Washington, D.C. 20546 Attn: Code RRM	(1)
NASA Lewis Research Center 21000 Brookpark Road Cleveland, Ohio 44135 Attn: Library	(1)
National Bureau of Standards Washington, D.C. 20234 Attn: Metallurgy Division Inorganic Materials Division	(1) (1)
Defense Metals and Ceramics Information Center Battelle Memorial Institute 505 King Avenue Columbus, Ohio 43201	(1)
Director Ordnance Research Laboratory P.O. Box 30 State College, Pennsylvania 16801	(1)
Director Applied Physics Laboratory University of Washington 1013 Northeast Fortieth Street Seattle, Washington 98105	(1)
Metals and Ceramics Division Oak Ridge National Laboratory P.O. Box X Oak Ridge, Tennessee 37380	(1)
Los Alamos Scientific Laboratory P.O. Box 1663 Los Alamos, New Mexico 87544 Attn: Report Librarian	(1)
Argonne National Laboratory Metallurgy Division P.O. Box 229 Lemont, Illinois 60439	(1)

Organization	No. of Copies	Organization	No. of Copies
Brookhaven National Laboratory Technical Information Division Upton, Long Island New York 11973 Attn: Research Library	(1)		
Library Building 50 Room 134 Lawrence Radiation Laboratory Berkeley, California 94720	(1)		

SUPPLEMENTARY DISTRIBUTION LIST October 1977

Technical and Summary Reports

Organization	No. of Copies
Dr. W.F. Adler Effects Technology Inc. 5383 Hollister Avenue P.O. Box 30400 Santa Barbara, CA 92105	(1)
Dr. G. Bansal Battelle Memorial Institute 505 King Avenue Columbus, OH 43201	(1)
Dr. R. Bratton Westinghouse Research Lab. Pittsburgh, PA 15235	(1)
Dr. A. G. Evans Rockwell International Corporation Science Center 1049 Camino Dos Rios, P.O. Box 1085 Thousand Oaks, CA 91360	(1)
Mr. E. H. Fisher Ford Motor Company Engineering & Research 12500 Oakwood Boulevard Dearborn, MI 48121	(1)
Dr. P. Gielisse University of Rhode Island Kingston, RI 02881	(1)
Dr. M.E. Gulden International Harvester Company Solar Division 2200 Pacific Highway San Diego, CA 92138	(1)
Dr. D.P.H. Hasselman Montana Energy and MHD Research and Development Institute P.O. Box 3809 Butte, Montana 59701	(1)
Mr. G. Hayes Naval Weapons Center China Lake, CA 93555	(1)
Professor A.H. Heuer Case Western Reserve University University Circle Cleveland, OH 44106	(1)
Dr. R. Hoagland Battelle Memorial Institute 505 King Avenue Columbus, OH 43201	(1)
Dr. R. Jaffee Electric Power Research Institute 3412 Hillview Avenue Palo Alto, CA 94304	(1)
Dr. P. Jorgensen Stanford Research Institute Poulter Laboratory Menlo Park, CA 94025	(1)
Dr. R. N. Katz Army Materials and Mechanics Research Center Arsenal Street Watertown, MA 02172	(1)
Dr. H. Kirchner Ceramic Finishing Company P.O. Box 498 State College, PA 16801	(1)
Dr. B. Koepke Honeywell, Inc. Corporate Research Center 500 Washington Avenue, South Hopkins, MN 55343	(1)
Mr. Frank Koubek Naval Surface Weapons Center White Oak Laboratory Silver Spring, MD 20910	(1)
Mr. E. H. Krafft Carborundum Company Research & Development P. O. Box 337 Niagara Falls, NY 14302	(1)

Organization	No. of Copies
Dr. F. F. Lange Rockwell International Corporation Science Center 1049 Camino Dos Rios, P.O. Box 1085 Thousand Oaks, CA 91360	(1)
Dr. J. Lankford Southwest Research Institute 8500 Culebra Road San Antonio, TX 78284	(1)
Library Norton Company Industrial Ceramics Division Worcester, MA 01606	(1)
State University of New York College of Ceramics at Alfred University Attn: Library Alfred, NY 14802	(1)
Dr. L. Hench University of Florida Ceramics Division Gainesville, FL 32601	(1)
Dr. N. MacMillan Materials Research Laboratory Pennsylvania State University College Park, PA 16802	(1)
Mr. F. Markarian Naval Weapons Center China Lake, CA 93555	(1)
Dr. Perry A. Miles Raytheon Company Research Division 28 Seyon Street Waltham, MA 02154	(1)
Mr. R. Rice Naval Research Laboratory Code 6360 Washington, D.C. 20375	(1)
Dr. J. Ritter University of Massachusetts Department of Mechanical Engineering Amherst, MA 01002	(1)
Professor R. Roy Pennsylvania State University Materials Research Laboratory University Park, PA 16802	(1)
Dr. R. Ruh AFML Wright-Patterson AFB Dayton, OH 45433	(1)
Mr. J. Schuldies AiResearch Manufacturing Company 4023 36th St., P.O. Box 5217 Phoenix, AZ 85010	(1)
Professor G. Sines University of California, Los Angeles Los Angeles, CA 90024	(1)
Dr. N. Tallan AFML Wright-Patterson AFB Dayton, OH 45433	(1)
Dr. T. Vasilos AVCO Corporation Research and Advanced Development Division 201 Lowell Street Wilmington, MA 01887	(1)
Mr. J.D. Walton Engineering Experiment Station Georgia Institute of Technology Atlanta, GA 30332	(1)
Dr. S.M. Widerhorn Inorganic Materials Division National Bureau of Standards Washington, DC 20234	(1)

Organization	No. of Copies
Dr. S.A. Bortz IITRI 10 W. 35th Street Chicago, IL 60616	(1)
Mr. G. Schmitt Air Force Materials Laboratory Wright-Patterson AFB Dayton, OH 45433	(1)
Dr. D.A. Shockey Stanford Research Institute Poulter Laboratory Menlo Park, CA 94025	(1)
Dr. W.G.D. Frederick Air Force Materials Laboratory Wright-Patterson AFB Dayton, OH 45433	(1)
Dr. P. Land Air Force Materials Laboratory Wright-Patterson AFB Dayton, OH 45433	(1)
Mr. K. Letson Redstone Arsenal Huntsville, AL 35809	(1)
Dr. S. Freiman Naval Research Laboratory Code 6363 Washington, DC 20375	(1)
Director Materials Sciences Defense Advanced Research Projects Agency 1400 Wilson Boulevard Arlington, VA 22209	(1)
Dr. James Pappis Raytheon Company Research Division 28 Seyon Street Waltham, MA 02154	(1)
Major W. Simmons Air Force Office of Scientific Research Building 410 Bolling Air Force Base Washington, DC 20332	(1)
Dr. P. Becher Naval Research Laboratory Code 6362 Washington, DC 20375	(1)
Mr. L.B. Weckesser Applied Physics Laboratory Johns Hopkins Road Laurel, MD 20810	(1)
Mr. D. Richarson AiResearch Manufacturing Company 4023 36th Street P.O. Box 5217 Phoenix, AZ 85010	(1)
Dr. H.E. Bennett Naval Weapons Center Code 3818 China Lake, CA 93555	(1)
Mr. G. Denman Air Force Materials Laboratory Code LPJ Wright-Patterson AFB Dayton, OH 45433	(1)
Dr. D. Godfrey Admiralty Materials Laboratory Polle, Dorset BH16 6JU UNITED KINGDOM	(1)
Dr. N. Corney Ministry of Defense The Adelphi John Adam Street London WC2N 6BB UNITED KINGDOM	(1)

Organization	No. of Copies
Dr. L.M. Gillin Aeronautical Research Laboratory P.O. Box 4331 Fisherman's Bend Melbourne, VIC 3001 AUSTRALIA	(1)
Dr. J. D. Buch Prototype Development Assoc., Inc. 1740 Garry Avenue, Suite 201 Santa Ana, CA 92705	(1)
Dr. B. Budiansky Harvard University Department of Engineering and Applied Science Cambridge, MA 02138	(1)
Professor H. Conrad University of Kentucky Materials Department Lexington, KY 40506	(1)
Dr. A. Cooper Case Western Reserve University Materials Department Cleveland, OH 44106	(1)
Professor John Field University of Cambridge New Cavendish Laboratory Cambridge, UNITED KINGDOM	(1)
Dr. I. Finney University of California Berkeley, CA 94720	(1)
Mr. A. A. Fyall Royal Aircraft Establishment Farnborough, Hants UNITED KINGDOM	(1)
Dr. L. Rubin Aerospace Corporation P. O. Box 92957 Los Angeles, CA 90009	(1)
Dr. R. A. Tanzilli General Electric Company Reentry and Environmental Systems Division 3198 Chestnut Street Philadelphia, PA 19101	(1)
Mr. T. Derkus TRW Cleveland, OH 44117	(1)
Dr. S. Hart Naval Research Laboratory Washington, D.C. 20375	(1)
Dr. B. R. Lawn Physics Department University New South Wales Kingston, New South Wales AUSTRALIA	(1)